

pubs.acs.org/cm Article

Vast Structural and Polymorphic Varieties of Semiconductors $AMM'Q_4$ (A = K, Rb, Cs, Tl; M = Ga, In; M' = Ge, Sn; Q = S, Se)

Daniel Friedrich, Shiqiang Hao, Shane Patel, Chris Wolverton, and Mercouri G. Kanatzidis*



ACCESS I

Cite This: Chem. Mater. 2021, 33, 6572-6583

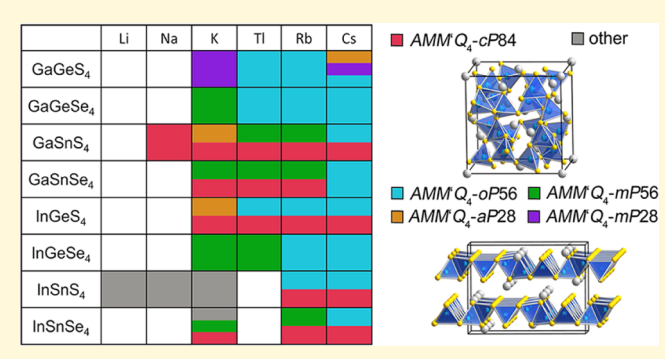


Article Recommendations

ABSTRACT: Nine new chalcogenide semiconductors AInM'Q₄ (A⁺ = K⁺, Rb⁺, Cs⁺, Tl⁺; M'⁴⁺ = Ge⁴⁺, Sn⁴⁺; Q²⁻ = S²⁻, Se²⁻) have been prepared by solid-state syntheses and structurally characterized by single-crystal X-ray diffraction techniques. These new phases fill in the missing links in these quaternary systems and crystallize in various two-dimensional layered polymorphs, while combinations containing large M³⁺ and M'⁴⁺ cations also adopt an extended three-dimensional (3D) network structure. The AMM'Q₄ materials exhibit a wide range of band gaps with colored selenides (1.8 eV < E_g < 2.3 eV) and mostly white sulfides (2.5 eV

 $< E_{\rm g} < 3.6$ eV). These phases have direct band gaps except for the thallium analogues and the cubic AGaSnSe₄-cP84. First-principles

III Metrics & More



Supporting Information

theoretical calculations of the electronic band structures reveal critical insight into the structure/property relationships of these materials. The distinct polymorphism of these quaternary phases is studied by discussing kinetic and thermodynamic factors responsible for the crystallization, structural considerations, and complementary density functional theory (DFT) calculations.

■ INTRODUCTION

Multinary chalcogenide semiconductors are a highly interesting class of materials because of their diverse optical properties. Among these, the quaternary compounds $A_a M_b M'_c Q_d$ (A = alkali metal, thallium; M = group 13 metal; M' = group 14 metal; Q = chalcogen) can exhibit strong nonlinear optical (NLO) second-harmonic generation (SHG) of noncentrosymmetric compounds like LiGaGe₂Q₆, $^{1-4}$ A₂In₂M'Q₆, $^{5-8}$ and TlGaSn₂Q₆. The centrosymmetric AGaM'Q₄ (A = K, Rb, Cs, Tl; M' = Si; Ge, Sn; Q = S, Se) phases have been reported to have high nonlinear optical (NLO) third-harmonic generation (THG) properties scaling inversely with the band gaps following a power-law behavior. 13 KInSn₂S₆ is capable of fast ion exchange for the capture of lanthanide ions. 14 Among compounds of the composition AMM'Q4 (A = K, Rb, Cs, Tl; M = Al; Ga, In; M' = Si; Ge, Sn; Q = S, Se), many have been experimentally isolated and characterized. 15-23 Most of these, however, do not simply crystallize in just one structure type but rather in various polymorphs with two-dimensional (2D) layered or three-dimensional (3D) network structures. Following our recent discovery of many new AGaM'Q4 phases and polymorphs, the present work focuses on the corresponding indium phases. We successfully managed to prepare and structurally characterize the remaining missing links of the AMM'Q₄ phases containing the heavier alkali metals potassium, rubidium, cesium, and thallium. Furthermore, we also managed to isolate new crystalline polymorphs of previously reported compositions. As of this work, a total of 52 different crystalline AMM'Q₄ phases have been reported

and almost all known combinations crystallize in more than one polymorphic modification. For this reason, we discuss this structural variety more in depth while presenting certain trends leading to the formation of the different polymorphs and complementary total energy density functional theory (DFT) calculations to study their stability. To properly distinguish between the crystalline polymorphs, the Pearson symbol (e.g., -cP84, -oP56, -aP28, etc.) is added at the end of the sum formula as a unique identifier, as suggested by the IUPAC and IUCr.²⁴ This symbol indicates the crystal system, lattice centering, and the number of atoms per unit cell, respectively. The optical properties of the new AInM'Q4 materials were also studied using optical absorption spectroscopy as well as firstprinciples quantum chemical density functional theory (DFT) calculations. A comprehensive study of all known AMM'Q4 polymorphs to date is also presented, which revealed a wide range of band gaps of these semiconductors, largely depending on the combination of the elements involved. Colored selenides absorb light in the infrared (IR)-green region (1.8 $eV < E_o < 2.3 eV$), while the mostly white sulfides absorb light in the blue-ultraviolet (UV) range (2.5 eV $< E_g < 3.6$ eV).

Received: June 26, 2021 Revised: July 20, 2021 Published: August 5, 2021





■ EXPERIMENTAL SECTION

Starting Materials. The commercially available elements potassium (K, Sigma-Aldrich, 99.95%), rubidium (Rb, Alfa Aesar, 99.5%), cesium (Cs, Alfa Aesar, 99.5%), thallium (Tl, Alfa Aesar, 99.99%) indium (In, Chempur, 99.999%), germanium (Ge, American Elements, 99.99%), tin (Sn, American Elements, 99.99%), sulfur (S, SN Plus, 99.999%), and selenium (Se, American Elements, 99.999%) were used as purchased without further purification. Alkali metal chalcogenides A_2Q (A = K, Rb, Cs; Q = S, Se) were prepared by reaction of the alkali metals with the respective chalcogens in liquid ammonia. ²⁵

Synthesis of the Title Compounds. All quaternary compounds discussed in this work were prepared by high-temperature solid-state reactions of stoichiometric proportions of the respective starting materials in evacuated fused silica tubes. In a typical 1.0 g batch, stoichiometric amounts of A2Q and other precursor materials were weighted in a fused silica tube (inner diameter 8 mm) in a nitrogenfilled glovebox. These tubes were evacuated to $\sim 10^{-4}$ mbar and flamesealed, and the 10-11 cm long tubes were placed in a programmable furnace and annealed according to the respective heating programs. The full details on the syntheses of compounds (1-9) and the respective temperature programs can be found in the Supporting Information. Phase purity and crystallinity of the solid products were determined by X-ray powder diffraction techniques after opening of the tubes, and all samples are single-phase solids unless stated otherwise. Single crystals of the materials were obtained from these batches by carefully crushing the sintered ingots/pellets obtained after the annealing into larger chunks and checking the surfaces for crystals under a microscope. As previously observed for the AGaM'Q4 phases, a general rule for the synthesis of AMM'Q4 compounds seems that the layered 2D polymorphs only form at high temperatures or after cooling of a molten batch, while the 3D network compounds need to be annealed below the melting point for an extended amount of time. It should also be noted that all sulfides are stable in moist air, while all selenides decompose within several minutes and release gaseous H₂Se while turning dark red and finally completely black. All selenides were therefore stored in a glovebox and only exposed to air for a minimal time before any characterization.

Single-Crystal X-ray Diffraction. Suitable single crystals of the title compounds were selected under a microscope and fixed to MiTeGen mounts using silicon grease. Ambient temperature diffraction data were collected on a Bruker Kappa APEX II diffractometer equipped with an I μ S microfocus X-ray (Mo-K α radiation, $\lambda = 0.71073$ Å) source and an APEX2 CCD detector. The resulting diffraction data were corrected for Lorentz and polarization effects. Absorption was corrected by a numerical absorption correction (based on the crystal faces) using the Bruker APEX II software suite. 26 All data sets had a completeness of 99.9% within 50° 2θ . The crystal structures were solved by intrinsic phasing methods using ShelXT2018/3 and refined on F2 with ShelXL2018/3 using fullmatrix least-squares methods. Further details on the crystal structure investigations may be obtained from the Fachinformationszentrum Karlsruhe, 76344 Eggenstein-Leopoldshafen, Germany (fax: (+49)7247-808-666; E-mail: crysdata@fiz-karlsruhe.de), on quoting the depository numbers CSD-2077324 for RbInSnSe₄-cP84 (1), CSD-2077323 for CsInSnSe₄-cP84 (2), CSD-2077327 for RbInGeS₄oP56 (3), CSD-2077328 for RbInGeSe₄ (4), CSD-2077322 for CsInSnS₄-oP56 (5), CSD-2077321 for CsInSnSe₄-oP56 (6), CSD-2077329 for KInGeSe₄ (7), CSD-2077326 for RbInSnSe₄-mP56 (8), and CSD-2077325 for TlInGeSe₄ (9).

The AInM' Q_4 compounds in this work have a mixed occupation of \ln^{3+} and M'^{4+} on all respective cation sites. The ideal ratio of \ln^{3+}/M'^{4+} has to be 1:1 for a charge-balanced AInM' Q_4 compound. Consequently, all initial structure refinements were performed with the assumption of an ideal equal occupancy of \ln^3 and \ln^{4+} or \ln^{4+} . The initial refinements of the cubic network structures with only one \ln^{3+}/M^{4+} cation site and the \ln^{3+}/S^{4+} compounds converged with good R values and low electron density maxima on the difference Fourier map. This was to be expected as \ln^{3+} and \ln^{3+} cannot be

distinguished using conventional single-crystal X-ray diffraction techniques. The initial refinements of the mixed In³+/Ge⁴+ compounds, however, converged with larger R values and large electron density maxima on the difference Fourier map. This indicated a preferred occupation of the cation sites with In³+ and Ge⁴+, respectively. This mixed occupation was treated by freely refining the occupation factors of the cation sites, and all resulting structure models converged with a total In³+/M⁴+ ratio of 1:1. All mixed In³+/Sn⁴+ sites still converged with marginal differences to the ideal composition, so the sites in these compounds were fixed at 50% occupancy for both cations. The mixed In³+/Ge⁴+ structures were refined with the least amount of restrictions possible, only using free variables for each site. All refinements converged with an ideal 1:1 ratio of In³+ and Ge⁴+ and a full occupancy of the A⁺ and Q²− sites, thus not requiring additional constraints like a SUMP command for charge balance.

The layered compounds AMM'Q₄-mP56 are very prone to stacking disorders resulting in twinned crystals. This appears to be an intrinsic phenomenon as all investigated crystals showed minor to severe signs of twinning. In the compounds KInGeSe₄ and RbInSnSe₄-mP56, significantly better solutions could be obtained by introducing a twin domain with a twin fraction of about 3%. These twin matrices were obtained with the TwinRotMat program of the PLATON software package.²⁷ The compound TlInGeSe₄, crystallizing in the same structure type, showed the most severe twinning of all our investigated gallium and indium AMM'Q4 phases. This is likely a result of the structure combined with additional disorder being introduced by the Tl+ lone pair. As only severely twinned crystals of the phase could be obtained, the structure was solved from a well-ordered nonmerohedrally twinned crystal with two twin domains and a twin fraction of 35%. Figure S8 shows reconstructed hkl planes as well as the axes of both twin domains of the measured crystal. The twinning matrix of the two domains was determined using the Cell Now program of the Bruker APEX II software suite. 28 Indexation and a twin absorption correction were performed by using the programs SAINT²⁹ in twinning mode and the TWINABS³⁰ program of the Bruker APEX II software suite.²⁶ The structure was solved from the prepared hklf5 file by intrinsic phasing methods using ShelXT2018/ 3^{31} and refined on F^2 with ShelXL2018/ 3^{32} using full-matrix leastsquares methods, and the resulting structure model converged with significantly better R values. Calculations of the volumes of the tetrahedra were performed with the program IVTON.3

Density Functional Theory (DFT) Calculations. DFT calculations within the generalized gradient approximation (GGA) were used to calculate the electronic structures of the title compounds. The Perdew–Burke–Ernzerhof exchange–correlation functional with projector-augmented wave potentials was applied to all calculations. The periodic boundary conditions and a plane-wave basis set were utilized as implemented in the Vienna ab initio simulation package. The total energies were numerically converged to approximately 3 meV/cation using a dense k-mesh, corresponding to 4000 k-points per reciprocal atom in the Brillouin zone, and a basis set energy cutoff of 500 eV. To find proper structure models for the mixed Ga³⁺/M'⁴⁺ occupation, the lowest-energy configuration was chosen from a vast number of geometrically distinct Ga³⁺/M'⁴⁺ possibilities. For the 10 structures with the lowest electrostatic energies, further DFT calculations were performed to identify the most favorable (lowest-energy) configuration.

■ RESULTS AND DISCUSSION

Crystal Structures. Most of the known AInM'Q₄ (A = K, Rb, Cs, Tl; M' = Ge, Sn; Q = S, Se)^{15,19} and AGaSnQ₄ (A = K, Rb, Cs, Tl; Q = S, Se)^{13,18} crystallize in a 3D network structure in the cubic space group $Pa\overline{3}$ (No. 205) with a unit cell parameter of $a \approx 13$ Å. The network structure found in these compounds is identical to the ternary phase BaGa₂S₄;³⁶ however, half of the Ga³⁺ cations in the structure are replaced by M'⁴⁺ (M' = Ge, Sn) cations, thus allowing only monovalent

 A^+ (A = alkali metal, Tl) cations for a charge-balanced structure. Basic crystallographic data for AInSnSe₄-cP84 (A = Rb, Cs) (1, 2) can be found in Table 1. The full details of the data collections, structure refinements, and interatomic distances can be found in the Supporting Information (Tables S1–S8).

Table 1. Crystallographic Data^a of the Cubic Network AInSnSe₄-cP84 Compounds

RbInSnSe ₄ -cP84 (1)	CsInSnSe ₄ -cP84 (2)	
Pa₃ (N	$Pa\overline{3}$ (No. 205)	
13.9728(1)	14.1932(3)	
2728.04(6)	2859.2(2)	
12		
4.637	4.755	
26.516	23.990	
20		
0.0571, 0.0152	0.0525, 0.0118	
0.0128, 0.0276	0.0130, 0.0274	
0.0148, 0.0284	0.0139, 0.0277	
-0.428, 0.462	-0.548, 0.701	
	Pa3 (N 13.9728(1) 2728.04(6) 1 4.637 26.516 2 0.0571, 0.0152 0.0128, 0.0276 0.0148, 0.0284	

^aThe full details of the data collection and structural refinement can be found in the Supporting Information.

The 3D network structure of these phases is composed of solely corner-sharing $(In/Sn)Se_4$ tetrahedra. For a better description, the extended structure can be regarded as stacked layers connected by common chalcogenide anions. A single layer is composed of corner-sharing $(In/Sn)_3Se_9$ tetrahedra triplets linked to four other building blocks by common corners. One such layer in the bc plane with atoms in the crystallographic a direction ranging from 0 < x < 0.5 is shown in Figure 1a. It should be noted that these directions can be exchanged accordingly as the structure crystallizes in a cubic centrosymmetric space group. The connection between these layers is realized by condensation of the two unconnected corners of one $(In/Sn)_3Se_9$ building block, each linking to one

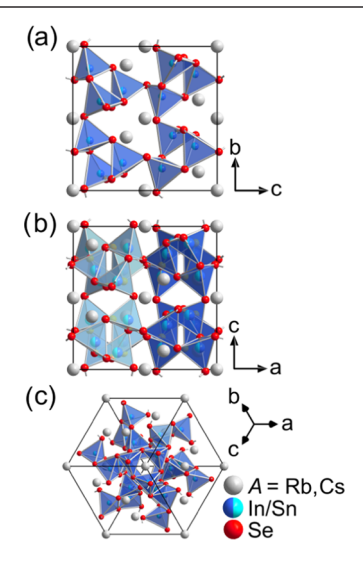


Figure 1. Crystal structure of the cubic 3D network structure showing (a) a section of one corner-sharing layer in the *bc* plane; (b) the extended structure when viewed along (010) with two layers highlighted by different shades of blue; and (c) the network structure viewed along (111).

adjacent layer, thus forming the $^3_{\infty}[InSnSe_4^{-}]$ network (Figure 1b.c).

The In³⁺ and Sn⁴⁺ cations occupy one mixed 24d site with 50% occupation of each cation in this structure type. The distances d(In/Sn-Se) in both compounds AInSnSe₄-cP84 (A = Rb, Cs) (1, 2) are almost identical in the range from 2.533(1) Å < d(In/Sn-Se) < 2.552(1) Å. The angles in these tetrahedra do not differ too much from the ideal tetrahedron angle of 109.5°. The A+ cations are located on two crystallographically independent sites in the cavities of the anionic network. The higher-symmetry 4a site located in the origin of the unit cell is coordinated by 12 Se²⁻ anions in a slightly distorted cuboctahedral environment with two unique distances of d(Rb-Se) = 3.858(1) Å and 3.885(1) Å and d(Cs-Se) = 3.917(1) Å and 4.028(1) Å. The lower-symmetry8c site is 6-fold-coordinated by Se²⁻ in a distorted octahedral coordination. Two distances observed in these octahedral are slightly smaller with values of d(Rb-Se) = 3.469(1) Å and 3.634(1) Å and d(Cs-Se) = 3.619(1) and 3.792(1) Å. Within a sphere of 4.2 Å, three additional Se²⁻ anions can be found. The observed interatomic distances are in good agreement with other related phases and the sum of the ionic radii d(In-Se) = 2.60 Å, d(Sn-Se) = 2.53 Å, $d(RbSe) \approx 3.6$ Å, and $d(\text{Cs-Se}) \approx 3.8 \text{ Å}.^{37}$ The ability of this ternary cubic BaGa₂S₄ structure type to accommodate isoelectronic but not isovalent elements in mixed occupation on a single crystallographic site to give the quaternary phases is a testament to its high stability. It has the potential to provide a large expansion in composition space by the elaboration of many possible isoelectronic substitutions. The previously reported quaternary isostructural phase β -K₂ZnSn₃S₈ involving divalent and tetravalent atoms is consistent with this expectation.³⁸

In addition to these 3D structures, other layered 2D AInM'Q4 phases and lower-symmetry polymorphs of RbInSnSe₄ and CsInSnSe₄ could also be isolated and structurally characterized. These layered structures are similar to the analogous AGaM'Q₄ (A = K, Rb, Cs, Tl; M'= Ge, Sn; Q = S, Se) and related indium phases. $^{15-23,39}$ The new AInM'Q₄ phases (3-9) crystallize in the two most common layered structure types observed for AMM'Q4 phases, which are structurally related to GeS₂-mP28, 40 the high-temperature modification of GeS2, but show a slightly different connectivity of the atoms. This relationship was discussed in more detail in our work on the gallium compounds, ¹³ and only the relevant structures will be discussed in this section. Basic crystallographic data for the new AInM'Se₄-oP56 (3-6) and AInM'Se₄-mP56 phases (7-9) can be found in Table 2. The full details of the data collections, structure refinements, and interatomic distances can be found in the Supporting Information (Tables S9-S36).

The phases AInM'Q₄-oP56 (A = Rb, Cs; M' = Ge, Sn; Q = S, Se) (3–6) crystallize in a 2D-layered structure in the orthorhombic space group Pnma (No. 62). The same structure was also reported for the analogous AMM'Q₄ compounds $CsInGeQ_4$ (Q = S, Se)^{15,17} and a series of AGaM'Q₄ compounds. The anionic layers found in these structures are composed of edge- and corner-sharing $(In/M')Q_4$ tetrahedra. For a better description, these layers can be regarded as corner-sharing tetrahedra chains, linked by edge-sharing $(In/M')_2Q_6$ double tetrahedra units perpendicular to the chain direction. Each of these linkers is connected to two consecutive tetrahedra in the chains by four common corners (Figure 2). For reasons of consistency, the cation sites in the

Table 2. Crystallographic Data of the Orthorhombic and Monoclinic Layered AInM'Q4 Compounds

	RbInGeS ₄ - $oP56$ (3)	RbInGeSe ₄ (4)	CsInSnS ₄ -oP56 (5)	CsInSnSe ₄ -oP56 (6)	KInGeSe ₄ (7)	RbInSnSe ₄ - <i>mP</i> 56 (8)	TlInGeSe ₄ (9)
space group		Pnma (No. 62)			$P2_1/c$ (No. 14)	
a/Å	17.3315(4)	17.9948(6)	18.0138(4)	18.6650(5)	7.6108(3)	7.8104(2)	7.586(1)
$b/ m \AA$	7.3884(2)	7.6908(3)	7.6238(2)	7.8976(2)	12.4473(6)	12.6533(2)	12.134(1)
c/Å	12.2463(3)	12.6003(6)	12.4332(3)	12.7340(4)	18.0896(8)	18.7062(5)	18.023(1)
$\beta/{ m deg}$	90	90	90	90	97.238(4)	96.297(3)	96.037(6)
$V/{ m \AA}^3$	1568.16(7)	1743.8(1)	1707.50(7)	1877.10(9)	1700.0(1)	1837.52(8)	1649.8(2)
Z	8	8	8	8	8	8	8
$ ho_{ m calcd}/ m g\cdot m cm^{-3}$	3.386	4.475	3.848	4.828	4.239	4.589	5.653
$\mu(\text{Mo-K}_{\alpha})/\text{mm}^{-1}$	13.836	28.190	10.705	24.361	23.700	26.244	42.739
T/°C				20			
$R_{ m int}$ R_{σ}	0.0506, 0.0239	0.0491, 0.0227	0.0537, 0.0212	0.0499, 0.0202	0.0534, 0.0308	0.0504, 0.0340	0.0499
R_1 , w R_2 $[I > 3\sigma(I)]$	0.0210, 0.0473	0.0313, 0.0613	0.0259, 0.0624	0.0219, 0.0529	0.0535, 0.1528	0.0307, 0.0775	0.0525, 0.1098
R_1 , w R_2 [all data]	0.0244, 0.0498	0.0397, 0.0650	0.0296, 0.0640	0.0237, 0.0541	0.0692, 0.1641	0.0366, 0.0825	0.0749, 0.1222
$\Delta ho_{ m min}$, $\Delta ho_{ m max}/{ m e}\cdot{ m \AA}^{-3}$	-0.623, 0.776	-0.881, 1.032	-0.922, 1.078	-1.295, 1.474	-1.898, 1.311	-1.205, 1.308	-2.289, 3.728

[&]quot;The full details of the data collection and structural refinement can be found in the Supporting Information.

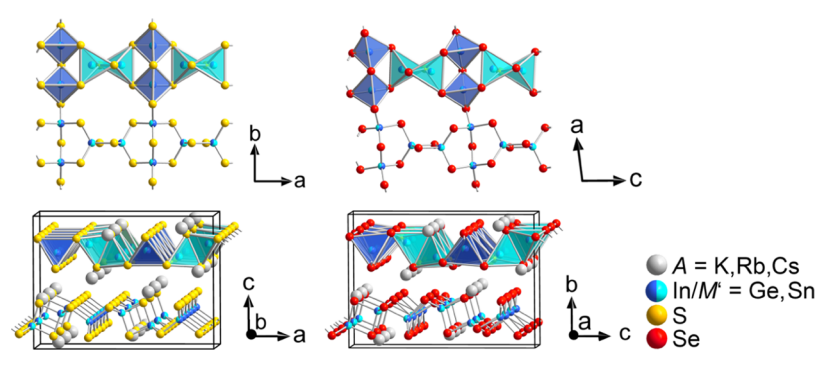


Figure 2. Crystal structures of the layered phases AMM' Q_4 -oP56 (left) and AMM' Q_4 -mP56 (right) showing (a, c) the connectivity of the polyhedral and atoms viewed perpendicular to the layers and (b, d) the unit cells of these phases viewed along the anionic layers.

 $({\rm In/M'})_2 Q_6$ linkers will be referred to as ${\rm In/M'1}$ and ${\rm In/M'2}$, and the sites forming the corner-sharing tetrahedra chain will be labeled ${\rm In/M'3}$ (site labels can also be found in Figure 2), analogous to our reported gallium compounds. The resulting layers in the structure run along the ab plane. The ${\rm In^{3+}}$ and ${\rm M'^{4+}}$ cations occupy three crystallographically independent sites, with ${\rm In/M'1}$ and ${\rm In/M'2}$ on special sites forming the $({\rm In/M'})_2 Q_6$ linkers and the ${\rm In/M'3}$ site solely forming the linear chains (for site labels, see Figure 2).

The distances d(In/M'-Q) in the tetrahedra vary with the differing connectivity of the tetrahedra among each other. Due to the connection to four adjacent tetrahedra solely by common edges, the distances in the In/M'3 are slightly longer with mean values of d(In/Ge-S) = 2.364(1)Å, d(In/Sn-S) =2.434(1) Å, $\bar{d}(In/Ge-Se) = 2.513(1)$ Å, and $\bar{d}(In/Sn-Se) =$ 2.541(1) Å. The distances d(In/M'1-Q) and d(In/M'2-Q) in the corner-sharing tetrahedra are slightly shorter with mean values of $\overline{d}(In/Ge-S) = 2.276(1) \text{Å}$, $\overline{d}(In/Sn-S) = 2.413(1) \text{Å}$, $\overline{d}(In/Ge-Se) = 2.405(1)$ Å, and $\overline{d}(In/Sn-Se) = 2.561(1)$ Å due to the difference in connectivity and each tetrahedron only being connected to three adjacent tetrahedra. Interestingly, the difference in the bond distances is significantly larger in the In/ Ge compounds compared to that in the In/Sn compounds. This likely results from the preferred occupation of the In/M'1 and In/M'2 sites with more M'4+ cations, which will be discussed in more detail in the next section. As a consequence of the differing connectivity, the distances d(In/M'-In/M')are also shorter in the edge-sharing linkers and longer in the

solely corner-sharing tetrahedra chains. The A⁺ cations (A = Rb, Cs) are found in the voids in between these anionic layers and occupy two crystallographically independent sites. Both these sites are 9-fold-coordinated by the chalcogenide anions within a sphere of 4.2 Å, and the resulting polyhedral cannot be attributed to a regular coordination polyhedron. The mean values of the distances d(A-Q) are $\overline{d}(Rb-S) = 3.696(1)$ Å, $\overline{d}(Cs-S) = 3.819(1)$ Å, $\overline{d}(Rb-Se) = 3.816(1)$ Å, and $\overline{d}(Cs-Se) = 3.929(1)$ Å.

The phases AInM'Se₄-mP56 (A = Rb, Cs, Tl; M' = Ge, Sn) (7-9) crystallize in a 2D-layered structure in the monoclinic space group $P2_1/c$ (No. 14). The same structure was also reported for KInSnSe₄, ¹⁹ KGaSnSe₄, ²⁰ RbGaSnSe₄-mPS6₄, ²⁰ and a series of AGaM'Q₄ compounds. ^{13,20} This structure features anionic layers with identical connectivity to the previously discussed AMM'Q4-oP56 phases; however, due to the reduced symmetry, the corner-sharing chains in these polymorphs are formed by two common crystallographic sites In/M'3 and In/M'4, rather than one special site (Figure 2). The decreased symmetry of the structure results in the layers becoming slightly distorted compared to the perfectly straight layers in the orthorhombic polymorphs (Figure 2). Similar to the orthorhombic, layered phases, the distances d(In/M'-Se)are longer in the double tetrahedra linkers, with mean values of $\overline{d}(In/Ge-Se) = 2.502(1) \text{ Å and } \overline{d}(In/Sn-Se) = 2.559(1) \text{ Å},$ compared to those of $\overline{d}(In/Ge-Se) = 2.412(1)$ Å and $\overline{d}(In/Ge-Se) = 2.412(1)$ Sn-Se) = 2.542(1) Å in the edge-sharing tetrahedra. These distances interestingly do not differ significantly from the

AMM'Q₄-oP56 phases, and minor differences can be attributed to the different A⁺ cations. Just like in the orthorhombic polymorphs, however, larger differences for the distances d(In/M'-Q) are observed in the In/Ge phases due to the preferred occupation of the cations, which will be discussed in the next section. In these monoclinic polymorphs, the A⁺ cations also occupy two crystallographically independent sites. These sites are still 9-fold-coordinated by the chalcogenide anions within a sphere of 4.2 Å; however, the coordination is more akin to a 7 + 2-fold coordination with seven shorter distances d(A-Q) < 4 Å and two slightly longer distances 4 Å < d(A-Q) < 4.2 Å. The mean values of the distances d(A-Q) with values of $\overline{d}(K-Se) = 3.580(1)$ Å, $\overline{d}(TI-Se) = 3.561(1)$ Å, and $\overline{d}(Rb-Se) = 3.705(1)$ Å are slightly shorter than in the orthorhombic polymorphs due to the slight change in the coordination.

Mixed Occupation of M³⁺ and M'⁴⁺. A problem during the refinement of the crystal structures of the new AInM'Q4 compounds was the occupation of the mixed cation sites with In³⁺ and Ge⁴⁺ or Sn⁴⁺. Like in the Ga/Ge phases, it is not possible to properly distinguish In³⁺ and Sn⁴⁺ using conventional X-ray diffraction techniques. Similar to our previously reported Ga/Ge phases, all occupation factors in the In/Sn compounds converged with an almost exact ratio of 1:1 and were therefore fixed to this ideal ratio. In the In³⁺/Ge⁴⁺ phases, the cations are not evenly distributed but prefer to occupy specific sites. Out of the sites that make up the anionic layers, the In/Ge1 and In/Ge2 sites and the In/Ge3 (and In/Ge4 sites in the monoclinic structures) basically have the same environment and connectivity, respectively. In general, the edge-sharing In/Ge1 and In/Ge2 tetrahedral sites are preferably occupied by the M'4+ cations, while the M³+ cations mostly occupy the corner-sharing In/Ge3 (and In/Ge4) site. Interestingly, for all four new compounds, almost identical values for the In3+ and Ge4+ occupation are observed, with \sim 75% In³⁺ on the In/Ge3 and In/Ge4 sites, 80% Ge⁴⁺ on the In/Ge1, and 60% Ge4+ on the In/Ge2. This difference in the occupation factors is also reflected in the bond lengths and volumes of the M/M'Q4 tetrahedra of all layered AMM'Q4 polymorphs, so this can be considered an intrinsic phenomenon for these layered phases. The average tetrahedra volumes, however, are very similar for a given combination of main group metals and chalcogens (Table S37).

Polymorphism and Stability of AMM'Q₄ Compounds. One fascinating fact about the AMM' Q_4 (A = Na, K, Rb, Cs, Tl; M = Ga, In; M' = Ge, Sn; Q = S, Se) is that almost all compositions crystallize in more than one structure type. This polymorphism results, e.g., in one given compound crystallizing in a 3D network structure or a 2D-layered structure. Even among the phases crystallizing solely in layered structure types, different structures (i.e., crystal symmetry) can be observed. As of this work, at least one crystalline structure of all possible combinations AMM' Q_4 (A = K, Rb, Cs, Tl; M = Ga, In; M' = Ge, Sn; Q = S, Se) has been reported. For the 32 different element combinations, a total of 52 different polymorphs have been reported. The only exceptions are $TlInSnQ_4$ (Q = S, Se), which rather form various solid solutions of Sn⁴⁺ in layered TlInQ₂ (TlGaSe₂ structure type).^{41–43} A similar situation has been reported for TlInGeSe₄. However, we still managed to isolate a quaternary phase from several batches. It should be noted, however, that these batches always contained small impurities of GeSe2, indicating that the formation of such stable quaternary thallium phases becomes more difficult as the atomic radii of the involved elements become larger. Figure 3

shows a schematic overview of all known quaternary AMM'Q₄ phases with the different polymorphs observed in each case.

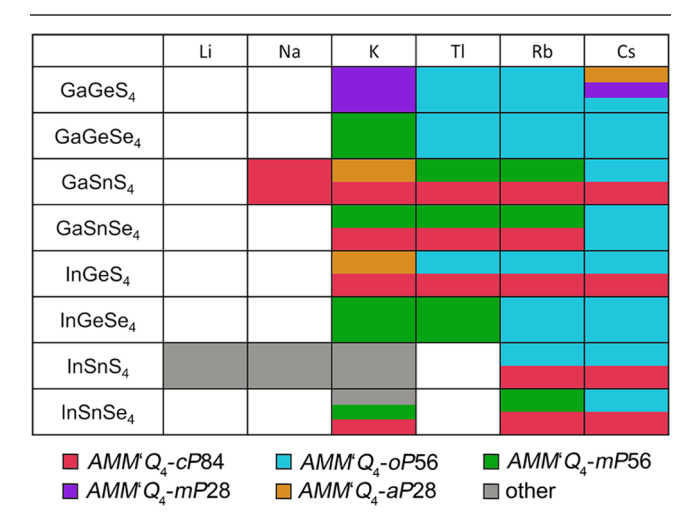


Figure 3. Schematic overview of all known AMM'Q₄ compounds sorted by the A⁺ cation size. The individual polymorphs are colorcoded: AMM'Q₄-cP84 (red), AMM'Q₄-oP56 (blue), AMM'Q₄-mP56 (green), AMM'Q₄-aP28 (orange), AMM'Q₄-mP28 (purple), AMM'Q₄-cP84 (red), and other (gray). Metastable quaternary phases obtained from ion-exchange reactions are excluded.

Most of the structure types observed for the AMM' Q_4 phases are two-dimensional; among them, the four most prominent are AMM' Q_4 -oP56, AMM' Q_4 -mP56, AMM' Q_4 -mP56, and AMM' Q_4 -aP28 polymorphs. For larger M³+ and M'⁴+ cations, 3D network polymorphs AMM' Q_4 -cP84 can also be observed. Due to this vast variety of structures, it is desirable to find certain trends to help better understand this structural variety, which could also be applied to other related systems. For this reason, we looked at thermodynamic/kinetic factors leading to the formation of certain polymorphs as well as geometrical considerations and theoretical DFT calculations for the stability of the individual phases.

One major example of the polymorphism of the AMM'O phases is the occurrence of the 3D network polymorphs AMM'Q₄-cP84. At first glance, it is apparent that this structure is only favored for larger M^{3+} and M^{4+} cations as at least one element from the fifth row of the periodic table must be present for this structure to be realized as no Ga/Ge phase could be isolated. The A+ cation appears to have no significant influence on the formation of these 3D network phases as they usually are observed for all A+ cations for a given combination of M³⁺/M'⁴⁺. Curiously, no AInGeSe₄-cP84 phase could be isolated either, despite all respective sulfides crystallizing in this structure type. This is likely a result of the large difference in the ionic radii of In³⁺ and Ge⁴⁺ of 43%, which is considerably larger than the difference of ~10% observed for all other combinations.³⁷ Apparently, the 3D network structure cannot be stabilized if there is a too large difference in the involved tetrahedra cations and a softer, more polarizable selenide environment, favoring other lower-symmetry polymorphs. These cubic 3D structures rarely are the only crystalline polymorph observed for a given element combination and only reproducibly form if a mixture is annealed for an extended amount of time below the melting point. This makes these polymorphs the thermodynamically controlled crystallization product in these systems.

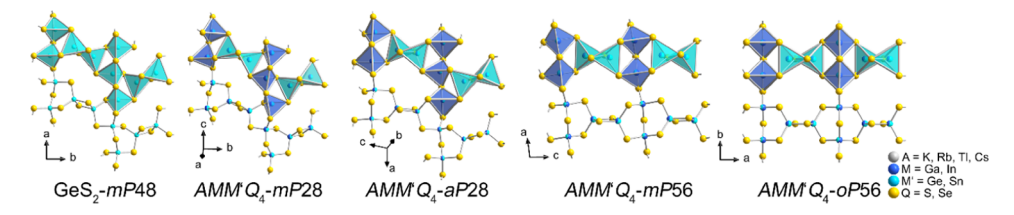


Figure 4. Comparison of the anionic layers in the four predominant layered AMM' Q_4 polymorphs and the layered high-temperature modification GeS₂-mP48. The preferred occupation of the mixed cation sites of M^{3+} and M^{4+} is color-coded with dark- and light blue-shaded tetrahedra, respectively. Differences in the connectivity of the atoms are highlighted by the red circles.

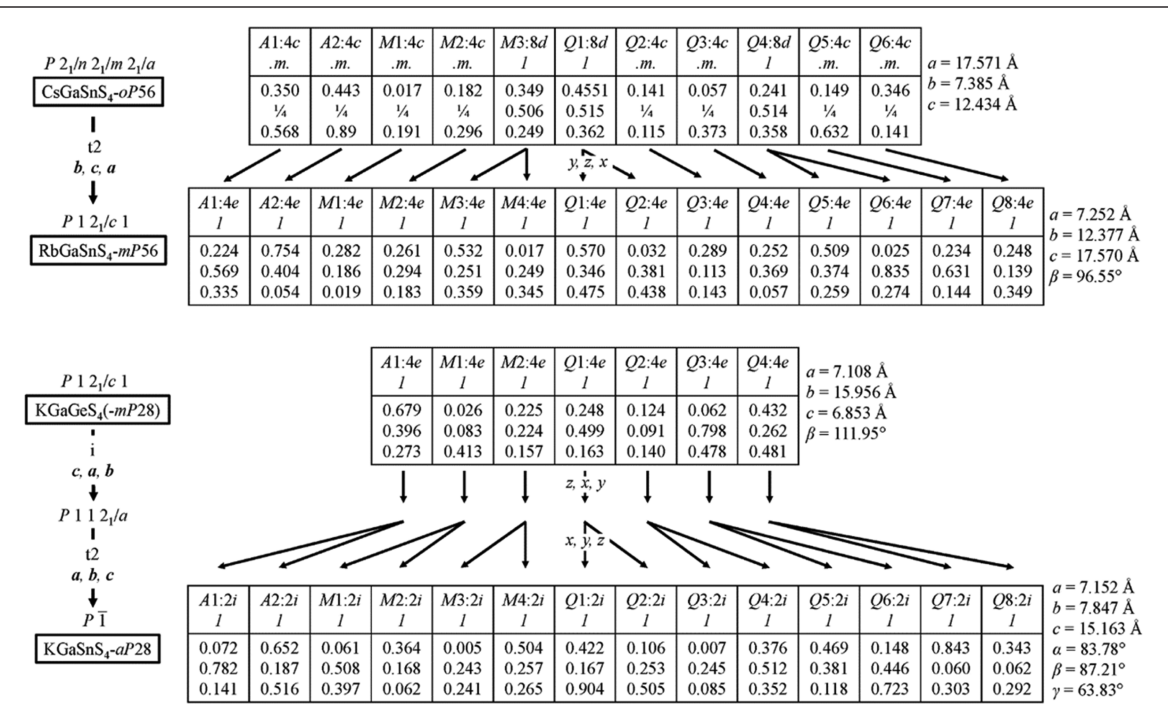


Figure 5. Bärnighausen trees showing the symmetry relations of the layered phases AMM'Q₄-oP56, AMM'Q₄-mP56, AMM'Q₄-mP28, and AMM'Q₄-aP28.

Melting of a quaternary mixture during the heat treatment and subsequent (slow) cooling of the batch lead to the crystallization of 2D-layered polymorphs rather than the 3D network structure. These layered phases are a kinetic crystallization product rather than the most thermodynamically stable structure. Besides the two layered polymorphs AMM'Q₄-oP56 and AMM'Q₄-mP56, which were already discussed for some of our newly characterized indium compounds, two additional layered phases, monoclinic AMM'Q₄-mP28 and triclinic AMM'Q₄-aP28, are also known. For these two polymorphs, however, significantly fewer examples with seemingly nonobvious trends have been reported. Figure 4 shows a comparison of the anionic layers observed in the four predominant layered polymorphs of the AMM'Q₄ compounds.

The four predominant layered structures of the AMM'Q₄ compounds are all related to the structure of the layered high-temperature modification of GeS_2 (GeS_2 -mP48 using the Pearson symbol). Substitution of half of the M'^{4+} cations with trivalent group 13 M^{3+} cations results in anionic layer $^2_{\infty}[MM'Q_4^{-}]$ with alkali metal countercations filling the voids in between the anionic layers to preserve charge balance. As discussed in the crystal structure part of this work, all of these layers are composed of condensed corner-sharing tetrahedra chains linked by edge-sharing Ge_2S_6 double tetrahedra units

perpendicular to the chain direction, with each linker being connected to two consecutive tetrahedra in the chain by four common corners. The connectivity of the atoms in a layer is identical in GeS₂-mP48 and the AMM'Q₄-mP28 and AMM'Q₄-aP28 polymorphs. In AMM'Q₄-mP56 and AMM'Q₄-oP56, a slight change in the connectivity in the anionic layers occurs, with the linkers no longer being staggered like in GeS₂-mP48 but perfectly aligned along a crystallographic axis. Monoclinic AMM'Q₄-mP56 can be considered a disordered version of orthorhombic AMM'Q₄-oP56, with the atoms in the corner-sharing chains being slightly displaced resulting in a slightly distorted look.

A look at our overview in Figure 3 reveals a clear trend for the two more prominent layered polymorphs AMM'Q₄-mP56 and AMM'Q₄-oP56. The monoclinic structure is mostly favored for smaller A⁺ cations, while the orthorhombic structure is mostly formed in compounds featuring large A⁺ cations. Furthermore, the disorder seems to be induced by the different sizes of the M³⁺ and M'⁴⁺ cations, which can be seen from the structure solutions of Ga/Sn and In/Ge compounds, which revealed that the M³⁺ cations preferably occupy the sites of the corner-sharing chain, while the M'⁴⁺ cations preferably occupy the edge-sharing double tetrahedra linkers.

These observations indicate that the larger, more polarizable, softer A^+ cations in the voids between the anionic layers can

compensate for this disorder, while the smaller, harder A+ cations are unable to compensate for this disorder. This effect leads to all cesium compounds crystallizing in the orthorhombic AMM'Q₄-oP56 and all potassium compounds crystallizing in the monoclinic AMM'Q4-mP56 structure type. For the rubidium and thallium phases, compounds containing tin favor the orthorhombic structure, while germanium compounds crystallize in the monoclinic structure. Liu et al. proposed a structure factor $F = r(M^{3+}) + r(M'^{4+}) +$ $2r(Q^{2-}) - 2r(A^{+})$, an equation of the ionic radii of the elements for the AGaSnS₄ (A = Rb, Cs) compounds. 45 If the value F for a given combination is larger than 1.6 Å, the compound will crystallize in the orthorhombic structure, while F < 1.6 Å will result in the monoclinic structure type. This equation holds true for some other AMM'Q4 combinations; however, it shows many exceptions.

The equation $F = [r(M^{3+}) + r(M'^{4+}) + r(Q^{2-})]/r(A^+)$ provides significantly better predictions whether a combination will result in the monoclinic or orthorhombic structure. Furthermore, using the ionic radii rather than the crystal radii results in values more in line with experimental results.³⁷ The observed threshold value of F is 1.85. Combinations while values above this threshold crystallize in the AMM'Q₄-mP56 structure and those below 1.85 crystallize in the AMM'Q₄-oP56 structure type. All of these calculated values can be found in the Supporting Information in Table S39. Using this equation for the AMM'Q₄-cP84 phases results in a broad range of values for F, so this equation can only be used for these layered phases. The same applies to the other layered polymorphs.

As previously stated, only few examples of AMM'Q₄-mP28 and AMM'Q₄-aP28 polymorphs are known, i.e., KGaGeS₄(-mP28), CsGaGeS₄-mP28, CsGaGeS₄-aP28, KGaSnS₄-aP28, and KInGeS₄-aP28. At first glance, it might appear that these low-symmetry structures are more favored for the smaller K⁺ cation. Our discovery of the polymorphs of CsGaGeS₄, however, indicates that this is not the case or only very specific combinations of these elements can form these stable polymorphs. While CsGaGeS₄-mP28 crystallizes isotypic to its potassium counterparts, a strong distortion of the anionic ²/_∞[GaGeS₄-] layers is observed in CsGaGeS₄-aP28, giving these layers a "wavy" look when viewed perpendicular to the layer. This change can possibly be attributed to the larger Cs⁺ cations requiring more space in between the layers, thus leading to this distortion.

A closer look at the structures of all layered phases revealed that these similar phases are also closely related crystallographically. Figure 5 shows the so-called Bärnighausen trees, 46 explaining the symmetry relations between AMM'Q₄-oP56 and AMM'Q4-mP56 as well as AMM'Q4-mP28 and AMM'Q4aP28. Using symmetry relations of the respective space groups, the atomic sites in AMM'Q4-oP56 can be converted to the sites observed in AMM'Q₄-mP56 by applying the matrix transformation (0 1 0, 0 0 1, 1 0 0) and subsequent splitting of each of the three 8d Wyckoff sites into two 4e sites. Similarly, the structure of AMM'Q4-mP28 can be converted by first transforming the structure to $P112_1/a$, an alternate setting of $P12_1/c1$, and subsequent splitting of each 4e Wyckoff site into two 2i sites, resulting in the triclinic structure of AMM'Q₄aP28. Smaller differences of the actual atomic coordinates can be attributed to different elements in these structures and the increasing degree of deformation in the layers with decreasing symmetry. It should be noted, however, that a direct

conversion of the structure of AMM' Q_4 -mP56 to AMM' Q_4 -mP28 is not possible as the necessary unit cell enlargement is not allowed without breaking the symmetry of $P2_1/c$. This is not too surprising as the connectivity in the anionic layers of these phases slightly differs.

For the lighter alkali metal cations, no quaternary phases besides LiInSnS₄, 15 crystallizing in the spinel structure, onedimensional tetragonal KGaSnSe₄ with SiS₂-type edge-sharing chains,²⁰ and a series of isotypic AInSnS₄ phases (A = Na, K) have been reported. 15 The structure of these layered phases is not related to the GeS2 structure but rather the layered SnS2 structure comprised edge-sharing SnS₆ octahedra. In these hexagonal AInSnS₄ phases, half of the Sn⁴⁺ cations in the octahedra are substituted by In^{3+} and the A^+ cations are located between the $^2_\infty[InSnS_4^{-}]$ layers to ensure chargebalanced phases. Due to the nature of these layered phases, ion exchange of the A+ cations in solutions is possible, and therefore, otherwise inaccessible isotypic phases of the heavier A+ cations Rb+, Cs+, and Tl+ can be obtained postsynthetically. To this date, this approach appears to be the only way to prepare Tl_aIn_bSn_cQ_d phases related to the title compounds, as solid-state reactions of the same stoichiometry always resulted in mixtures of SnQ_2 and solid solutions $Tl_{1-x}In_{1-x}Sn_xQ_2$. This structure type is limited to In/Sn phases, a result of the similar ionic radii of In³⁺ and Sn⁴⁺.

Electronic Structure Calculations, Phase Stability, and Optical Properties. Complementary DFT calculations used to predict the most stable quaternary AMM'Q4 polymorphs were also performed. The mixed M^{3+}/M^{4+} site was modeled for a vast number of distinct possibilities, and the most favorable (lowest-energy) configuration was identified from the 10 structures with the lowest energies. Calculations of the relative stability of the five most common AMM'Q4 polymorphs (-cP84, -oP56, -mP56, -mP28, and -aP28) should reveal the thermodynamically most stable polymorph for a given element combination. The calculations provide more insight to develop a potential tool to predict the not-yetisolated polymorphs. Table S40 lists the values obtained from the total energy calculations of all element combinations for these five most common polymorphs. Figure 6 shows a plot of the total energies for all element combinations for the different polymorphs.

In all cases, the total energy calculations reveal one experimentally isolated phase as the most stable polymorph. In most cases, the thermodynamic crystallization product is also the lowest-energy structure or only marginally less stable. The calculations correctly predict the 3D network structure AMM'Q₄-cP84 as the lowest-energy structure in most cases but also correctly identify layered phases as more stable for CsGaSnSe₄, AGaGeQ₄, and AInGeSe₄. In quaternary systems with a thermodynamic 3D network structure and a kinetic layered polymorph, the correct experimentally isolated layered phase is usually predicted to be the second lowest-energy structure. For CsGaGeS4, the orthorhombic polymorph CsGaGeS₄-oP56 is also identified as the thermodynamic product, while the lower-symmetry polymorphs CsGaGeS₄mP28 and CsGaGeS₄-aP28 are only predicted to be slightly less stable. While the total energies for the polymorphs are all relatively close, the monoclinic layered phases AMM'Q4 are always calculated to have much higher total energies than all other polymorphs. This behavior appears to be a systematic issue for these calculations. All in all, the experimental results prove that the performed total energy calculations can

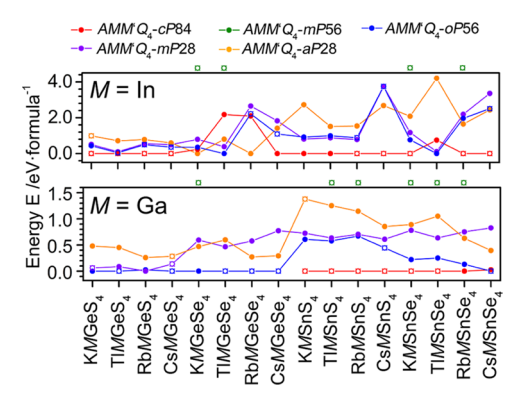


Figure 6. Plot of the total energies of different polymorphs for all AMM'Q₄ combinations. The values are normalized to the lowest value for each composition. Experimentally isolated polymorphs are represented by open circles. The values for AMM'Q₄-mP56 polymorphs are at higher values (10 eV/formula unit and above) and are therefore excluded from this graph unless the polymorph is experimentally confirmed. For the gallium compounds, no -cP84 values are shown as there is no experimental proof of any gallium phase crystallizing in this structure type.

accurately determine stable polymorphs in complex systems and are a valuable tool for the targeted discovery of new phases in seemingly well-examined systems.

The optical absorption data for compounds 1–9 and the determined band gaps are shown in Figure S9 in the Supporting Information. Figure 7 shows an overview of the trends of the optical absorption edges observed for different element combinations for the layered and cubic phases. Band structure plots of the most important structure types and combinations are shown in Figure 8. Similar to our reported

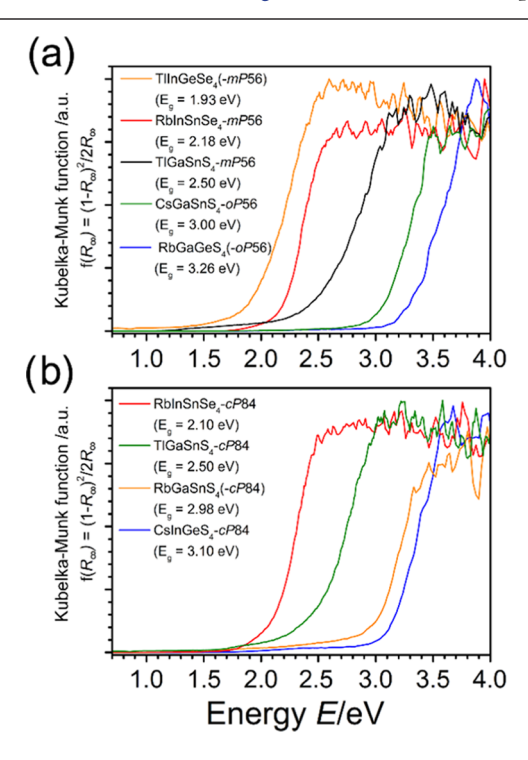


Figure 7. UV/vis absorption spectra of selected layered (a) and cubic network (b) AMM' Q_4 phases showing the diversity of optical band gaps varying with the element combinations. The experimental bandgap values are given in the legends.

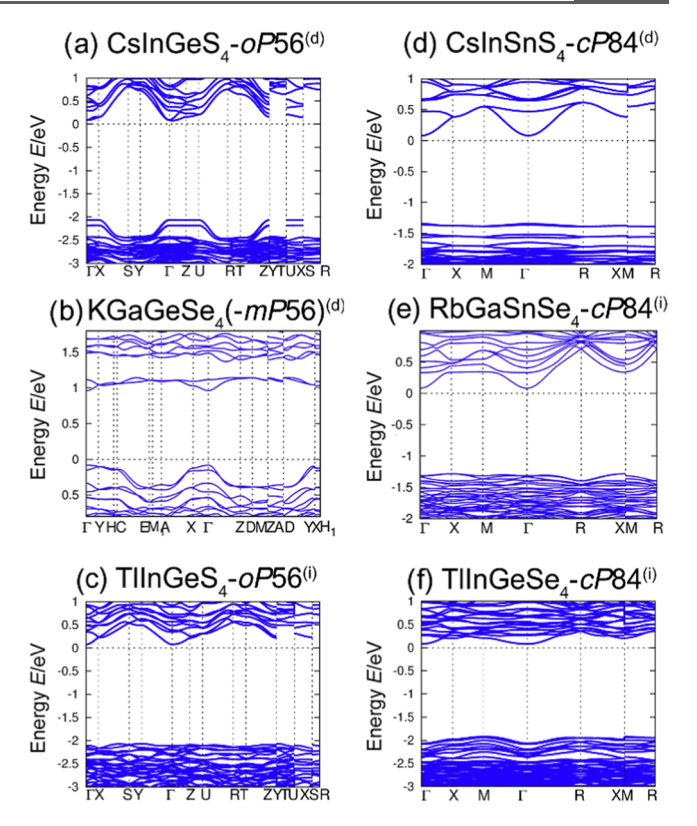


Figure 8. Band structure plots of selected AMM' Q_4 phases. Layered phases are listed on the left side (a–c), and 3D network phases are listed on the right side (d–f). The band-gap types direct (d) and indirect (i) are also indicated.

gallium compounds and related AMM' $\mathrm{Q_4}$ semiconductors, a clear trend for the band gaps of the respective sulfides and selenides can be observed. The selenides have significantly smaller band gaps (1.5 eV < E_{g} < 2.6 eV) than the sulfides (2.3 eV < E_{g} < 3.6 eV). For a comprehensive overview, all experimentally determined band gaps of AMM' $\mathrm{Q_4}$ semiconductor polymorphs reported to date are listed in Table 3. Missing and questionable band-gap data were remeasured for confirmation and the sake of completeness (Figure S10). A table of the band gaps sorted by their values can be found in the Supporting Information (Table S41).

For the alkali metal compounds, only marginal differences in the reported band-gap values are observed for a given structure type and element combination. Substitution of the alkali metal A⁺ does not significantly influence the band-gap values, which is consistent with the fact that the alkali metal states do not contribute to the states close to the Fermi level in these and related compounds. ^{1,4,9,11,13,45,48} However, a red shift of the band gaps for the thallium sulfide compounds, compared to that for their alkali metal counterparts, can be observed, which likely results from the contributions of the electronic states of the Tl⁺ lone pair and empty p-states leading to a shrinking of the band gaps.

To gain further insight into the electronic structures of these solids, complementary DFT calculations were performed. As noticed for the respective gallium compounds that the electronic structures are not affected by the alkali metal substitution for a given structure type, only one representative of an alkali metal compound for a given structure was calculated. The band structures and density of states (DOS) for these compounds can be found in the Supporting

Table 3. Optical Band-Gap Values $E_{\rm g}/{\rm eV}$ of All Compounds 1–9 and All Other AMM'Q₄ Semiconductor Polymorphs Reported to Date^a

		1 1			1 1
compound	type	band gap $E_{ m g}/{ m eV}$	compound	type	band ga E _g /eV
KGaSnS ₄ - aP28	d	2.60 ¹³	KInGeS ₄ -aP28	d	3.34 ^b
CsGaGeS ₄ - aP28	d	3.01 ^b			
			KInGeSe ₄ (7)	d	2.32^{b}
KGaGeS ₄ - mP28	d	3.56 ¹³	$TlInGeSe_4$ (9)	i	1.93 ^b
CsGaGeS ₄ - mP28	d	no data	KInSnSe ₄ -mP56	d	1.80 ¹⁹
			RbInSnSe ₄ - mP56 (8)	d	2.18 ^b
KGaGeSe ₄	d	2.32^{13}			
TlGaSnS ₄ - mP56	i	2.50 ¹³	TlInGeS ₄ -oP56	i	$2.09,^{23}$ 2.30^{15b}
RbGaSnS ₄ - mP56	d	2.96 ⁴⁵	RbInGeS ₄ - <i>oP</i> 56 (3)	d	3.33 ^b
KGaSnSe ₄ - mP56	d	1.73 ¹³	CsInGeS ₄ -oP56	d	2.95, ¹⁵ 3.23 ^b
TlGaSnSe ₄ - mP56	i	1.95 ¹³	RbInGeSe ₄ (4)	d	2.2 ^b
RbGaSnSe ₄ - mP56	d	2.60 ¹³	$CsInGeSe_4$	d	2.3 ^{17b}
			RbInSnS ₄ -oP56	d	2.4 ¹⁵
$TlGaGeS_4$	d	2.71 ^{13,23}	CsInSnS ₄ -oP56 (5)	d	2.92 ^b
${\rm RbGaGeS_4}$	d	3.26 ¹³	CsInSnSe ₄ -oP56 (6)	d	2.15 ^b
CsGaGeS ₄ - oP56	d	3.18 ¹³			
TlGaGeSe4	i	2.21^{13}	KInGeS ₄ -cP84	d	3.10^{15}
CsGaGeSe₄	d	2.14^{13}	TlInGeS ₄ -cP84	i	2.30^{15}
CsGaSnS ₄ - oP56	d	3.07 ^{13,45}	RbInGeS ₄ -cP84	d	3.10 ¹⁵
CsGaSnSe ₄	d	1.97^{13}	CsInGeS ₄ -cP84	d	3.10^{15}
			RbInSnS₄-cP84	d	2.7^{15}
KGaSnS ₄ - cP84	i	2.10 ¹⁸	CsInSnS ₄ -cP84	d	2.9 ¹⁵
TlGaSnS ₄ - cP84	i	2.50 ¹³	KInSnSe ₄ -cP84	d	1.49 ¹⁹
RbGaSnS ₄ - cP84	d	2.98 ^{13,18}	RbInSnSe ₄ - <i>cP</i> 84 (1)	d	2.10 ^b
CsGaSnS ₄ - cP84	d	3.00 ^{13,18,45}	CsInSnSe ₄ - <i>cP</i> 84 (2)	d	2.02 ^b
KGaSnSe ₄ - cP84	i	2.10 ¹³			
TlGaSnSe ₄ - cP84	i	1.84 ¹³			
RbGaSnSe ₄ - cP84	i	1.88 ¹³			
a					

^aThese values are sorted by the respective structure types for gallium (left column) and indium compounds (right column). The band-gap type (direct or indirect) and respective references are also given for each compound. ^bMissing or uncertain data remeasured for this work, which can be found in the Supporting Information.

Information (Figures S11–S22). These calculations, our previously reported calculations for the gallium compounds, 13 and other DFT calculations performed on these compounds 1,4,9,11,13,45,48 are very consistent and revealed that all of the quaternary AMM' Q_4 phases are semiconductors. Differences between the experimental and calculated bandgap values may result from a different $\rm M/M^\prime$ disorder used for the calculations compared to those of the real compounds.

Furthermore, the calculated band-gap values usually underestimate the band gaps due to the insufficient description of the electronic states when using the GGA approximation. The states below the Fermi level in the AMM'Q4 phases are always dominated by the p-states of the respective chalcogens (S 3p, Se 4p) and the group 13 metals (Ga 4p, In 5p). For the thallium compounds, the Tl-6s lone-pair states also contribute to the highest states of the valence band. The alkali metal states s-states do not contribute to the states close to the Fermi level and are usually located below -8 eV. Above the Fermi level, contributions of the chalcogen p-states (S 3p, Se 4p), the group 14 metal s-states (Ge 4s, Sn 5s), and minor contributions of the group 14 metal p-states (Ge 4p, Sn 5p) can be found. The DOS of all AMM'Q4 compounds shows nonbonding Q²⁻ p-states and the antibonding M'⁴⁺ s-states cleanly separated below and above the Fermi level, thus leading to the optical absorption. The band-gap types (direct or indirect) calculated for all of the AMM'Q4 phases are also listed in Table 3. For a given structure type, the band-gap type is not consistent but rather changes with the combination of the elements involved. However, some trends, especially regarding the chalcogenides, are involved and the respective thallium analogues can be observed for a given structure type.

Among the 3D cubic structures AMM'Q4-cP84, all sulfides have a direct band gap. For the gallium selenides, however, indirect band gaps are observed. Considering that only Ga/Sn phases crystallize in this structure type, this change likely results from the relative differences in energy of the Ga states to the Ge and Sn states compared to those of its indium counterparts among the selenides. The isotypic thallium compounds also exhibit an indirect band gap, which can be attributed to the influence of the Tl-6s lone-pair states to the highest states of the valence band. The orthorhombic layered polymorphs AMM'Q₄-oP56 all have a direct band gap with the exception of the thallium compounds TlGaGeSe4 and TlInGeS₄-oP56, which again can be attributed to the influence of the Tl-6s states of the lone pair. All of the other layered AMM'Q₄ solids, triclinic AMM'Q₄-aP28, monoclinic AMM'Q₄-mP28, and monoclinic AMM'Q₄-mP56, containing alkali metal cations also have direct band gaps. The thallium phases TlMM'Q₄-mP56 again have an indirect band gap, a result of the contributions of the Tl-6s lone-pair states. All in all, these results reveal that a band-gap type is usually dominant for a given structure type and deviations from this trend are mostly observed for the respective thallium compounds.

Beyond the band structures, we further evaluated the effective masses of the six materials shown in Figure 8. For the density-of-state effective mass, we use $m_d^* = (g^2 \cdot m_{kx} \cdot m_{ky})$ m_{k_2})^{1/3}. The detailed electron and hole effective masses are listed in Table 4, and the results for the electron effective masses are within expected values. For the layered material CsInGeS₄-oP56, it is reasonable that the hole effective mass $(14.1 m_0)$ is much larger than for its 3D network analogue CsInSnS₄-cP84 (3.11 m_0) due to the very high contributions of the G-X and G-Z directions. For layered KGaGeSe₄-mP56 and TlInGeS₄-oP56, the hole density-of-state effective masses are 2.97 m_0 and 7.45 m_0 , respectively. Both these values are lower than those for their cubic 3D analogues RbGaSnSe₄cP84 (6.56 m_0) and TlInGeSe₄-cP84 (8.07 m_0). For the effective mass along a specific crystallographic direction, e.g., the a direction in KGaGeSe₄-mP56, a very large value m_{kx} *= 8.01 m_0 is obtained, which is much larger than that in any direction of cubic phase of RbGaSnSe₄-cP84. However, if we

Table 4. Calculated Values for the Effective Masses of Electrons m_e^* and Holes m_e^* in the Compounds Shown in Figure 8

compound	effective mass electron m_e^*/m_0	effective mass hole m_h^*/m_0
CsInGeS ₄ -oP56	0.66	14.1
KGaGeSe ₄ (- mP56)	1.21	2.97
TlInGeS ₄ -oP56	0.69	7.45
CsInSnS ₄ -cP84	0.33	3.11
RbGaSnSe ₄ -cP84	0.32	6.56
TlInGeSe ₄ -cP84	0.89	8.07

take a high degeneracy factor g=6 for the cubic phases and a low g=1 for the layered phases into account, the overall density-of-state effective mass for the layered material is even lower than that of the cubic phase. Thus, the higher symmetry of the cubic materials, in general, leads to overall higher effective masses even though layered materials exhibit higher values along specific crystallographic directions. Coupled with the fact that some of these semiconductors are direct band gap, this will have implications on phase selection from this family of compounds for specific device applications.

CONCLUSIONS

The nine new phases of AInM'Q₄ (A = K, Rb, Cs, Tl; M' = Ge, Sn; Q = S, Se) constitute the hitherto missing links among the heavier alkali metal AMM' Q_4 (M = Ga, In) compounds. We furthermore isolated new crystalline polymorphs of previously reported compounds, thus expanding the structural and compositional varieties of the AMM'Q4 family. We find that the formation of the cubic 3D structures AMM'Q₄-cP84 seems to be favored by thermodynamic parameters, while the various 2D-layered AMM'Q4 phases appear to be a kinetic product. Given that a few polymorphs cannot reliably be reproduced, they show that the competing thermodynamic and kinetic parameters are not yet fully understood and some phases might only form under very specific conditions. A more in-depth analysis of the various polymorphs of these quaternary phases revealed certain trends leading to the crystallization of specific structures. The cubic network phases AMM'Q₄-cP84 are only observed if at least one M or M' cation from the fifth row of the PSE is present. These cubic structures also represent the thermodynamic crystallization product as they reproducibly form only upon long annealing below the melting point. For each combination of elements with an AMM'Q4-cP84, there also always exists at least one of several 2D-layered polymorphs crystallizing as kinetic products when (slow)cooling a molten batch. Structural considerations revealed a trend of compounds with smaller $A^{\scriptscriptstyle +}$ and $M^{3\scriptscriptstyle +}/M^{\prime 4\scriptscriptstyle +}$ cations of similar size preferably crystallizing in the slightly disordered monoclinic AMM'Q4-mP56 polymorphs, while larger A+ cations lead to the ordered orthorhombic AMM'Q4-oP56 structure type. DFT calculations on the relative stability of these phases also predict the correct most stable phases and serve as a useful tool for the prediction of new compounds. All AMM'Q4 chalcogenides are semiconductors with a wide range of band gaps, depending on the combination of the elements. The density-of-state effective masses of these compounds are within expected values with the hole effective masses for the 3D compounds but it is unusual that they are generally higher than for the layered phases. The AMM'Q4

phases exhibit excellent high thermal and optical stabilities and have predominantly direct band gaps in the UV and vis regions. Analogous layered thallium compounds and cubic 3D network polymorphs $AGaM'Q_4$ -cP84 have indirect optical band gaps in the vis region, thus making them promising candidate materials for various optoelectronic applications.

ASSOCIATED CONTENT

Supporting Information

The Supporting Information is available free of charge at https://pubs.acs.org/doi/10.1021/acs.chemmater.1c02211.

Details on the single-crystal data collection, atomic parameters, displacement parameters, and interatomic distances for compounds 1–9; DTA analysis for compounds 1–9; reconstructed *hkl* planes of twinned TlInGeSe₄; tetrahedra volumes for all AMM'Q₄ compounds; values for the structure factor *F* for AMM'Q₄-oP56 and -mP56 polymorphs; calculated total energy values for all AMM'Q₄ combinations for the five polymorphs; optical band gaps sorted by ascending values; UV/vis absorption spectra for compounds 1–9 and other AMM'Q₄ compounds from the literature; and band structure and DOS plots for AInM'Q₄ compounds (PDF)

Crystallographic data (ZIP)

AUTHOR INFORMATION

Corresponding Author

Mercouri G. Kanatzidis — Department of Chemistry, Northwestern University, Evanston, Illinois 60208, United States; orcid.org/0000-0003-2037-4168; Email: mkanatzidis@northwestern.edu

Authors

Daniel Friedrich — Department of Chemistry, Northwestern University, Evanston, Illinois 60208, United States;
orcid.org/0000-0001-6953-8114

Shiqiang Hao — Department of Materials Science and Engineering, Northwestern University, Evanston, Illinois 60208, United States; orcid.org/0000-0002-7985-4468

Shane Patel – Department of Materials Science and Engineering, Northwestern University, Evanston, Illinois 60208, United States

Chris Wolverton – Department of Materials Science and Engineering, Northwestern University, Evanston, Illinois 60208, United States; orcid.org/0000-0003-2248-474X

Complete contact information is available at: https://pubs.acs.org/10.1021/acs.chemmater.1c02211

Author Contributions

The manuscript was written through contributions of all authors. All authors have given approval to the final version of the manuscript.

Notes

The authors declare no competing financial interest.

ACKNOWLEDGMENTS

This work was supported mainly by the National Science Foundation Grant DMR-2003476. D.F. would like to thank the German Research Foundation (DFG) for financial support (reference number: FR 4094/1-1).

REFERENCES

- (1) Mei, D.; Yin, W.; Feng, K.; Lin, Z.; Bai, L.; Yao, J.; Wu, Y. LiGaGe2Se6: A New IR Nonlinear Optical Material with Low Melting Point. *Inorg. Chem.* **2012**, *51*, 1035–1040.
- (2) Kim, Y.; Seo, I.; Martin, S. W.; Baek, J.; Shiv Halasyamani, P.; Arumugam, N.; Steinfink, H. Characterization of New Infrared Nonlinear Optical Material with High Laser Damage Threshold, Li₂Ga₂GeS₆. Chem. Mater. **2008**, 20, 6048–6052.
- (3) Yelisseyev, A. P.; Isaenko, L. I.; Krinitsin, P.; Liang, F.; Goloshumova, A. A.; Naumov, D. Y.; Lin, Z. Crystal Growth, Structure, and Optical Properties of LiGaGe₂Se₆. *Inorg. Chem.* **2016**, 55, 8672–8680.
- (4) Mei, D.; Zhang, S.; Liang, F.; Zhao, S.; Jiang, J.; Zhong, J.; Lin, Z.; Wu, Y. LiGaGe₂S₆: A Chalcogenide with Good Infrared Nonlinear Optical Performance and Low Melting Point. *Inorg. Chem.* **2017**, *56*, 13267–13273.
- (5) Li, S.-F.; Liu, B.-W.; Zhang, M.-J.; Fan, Y.-H.; Zeng, H.-Y.; Guo, G.-C. Syntheses, Structures, and Nonlinear Optical Properties of Two Sulfides Na₂In₂MS₆ (M = Si, Ge). *Inorg. Chem.* **2016**, *55*, 1480–1485.
- (6) Yin, W.; Feng, K.; Hao, W.; Yao, J.; Wu, Y. Synthesis, Structure, and Properties of $\text{Li}_2\text{In}_2\text{MQ}_6$ (M = Si, Ge; Q = S, Se): A New Series of IR Nonlinear Optical Materials. *Inorg. Chem.* **2012**, *51*, 5839–5843.
- (7) Yohannan, J. P.; Vidyasagar, K. Syntheses and structural characterization of non-centrosymmetric $Na_2M_2M'S_6$ (M, M' = Ga, In, Si, Ge, Sn, Zn, Cd) sulfides. *J. Solid State Chem.* **2016**, 238, 147–155.
- (8) Zhou, M.; Li, C.; Li, X.; Yao, J.; Wu, Y. K₂Sn₂ZnSe₆, Na₂Ge₂ZnSe₆, and Na₂In₂GeSe₆: a new series of quaternary selenides with intriguing structural diversity and nonlinear optical properties. *Dalton Trans.* **2016**, *45*, 7627–7633.
- (9) Vu, T. V.; Lavrentyev, A. A.; Gabrelian, B. V.; Tong, H. D.; Parasyuk, O. V.; Khyzhun, O. Y. Electronic band structure and basic optical constants of TlGaSn₂Se₆, a promising NLO semiconductor: First-principles calculations under DFT framework. *Optik* **2019**, *181*, 673–685.
- (10) Vu, T. V.; Lavrentyev, A. A.; Gabrelian, B. V.; Parasyuk, O. V.; Khyzhun, O. Y. TlInGe2S6, A Prospective Nonlinear Optical Material: First-Principles DFT Calculations of the Electronic Structure and Optical Properties. *J. Electron. Mater.* **2018**, 47, 5525–5536.
- (11) Vu, T. V.; Lavrentyev, A. A.; Gabrelian, B. V.; Parasyuk, O. V.; Khyzhun, O. Y. First-principles DFT calculations of the electronic structure and optical properties of TlInGe₂Se₆, a prospective NLO material. *Mater. Chem. Phys.* **2018**, 219, 162–174.
- (12) Parasyuk, O. V.; Babizhetskyy, V. S.; Khyzhun, O. Y.; Levytskyy, V. O.; Kityk, I. V.; Myronchuk, G. L.; Tsisar, O. V.; Piskach, L. V.; Jedryka, J.; Maciag, A.; Piasecki, M. Novel Quaternary TlGaSn₂Se₆ Single Crystal as Promising Material for Laser Operated Infrared Nonlinear Optical Modulators. *Crystals* **2017**, *7*, No. 341.
- (13) Friedrich, D.; Byun, H. R.; Hao, S.; Patel, S.; Wolverton, C.; Jang, J. I.; Kanatzidis, M. G. Layered and Cubic Semiconductors AGaM'Q4 (A+ = K+, Rb+, Cs+, Tl+; M'4+ = Ge4+, Sn4+; Q2- = S2-, Se2-) and High Third-Harmonic Generation. *J. Am. Chem. Soc.* **2020**, *142*, 17730–17742.
- (14) Xiao, C.; Hassanzadeh Fard, Z.; Sarma, D.; Song, T.-B.; Xu, C.; Kanatzidis, M. G. Highly Efficient Separation of Trivalent Minor Actinides by a Layered Metal Sulfide (KInSn₂S₆) from Acidic Radioactive Waste. *J. Am. Chem. Soc.* **2017**, *139*, 16494–16497.
- (15) Yohannan, J. P.; Vidyasagar, K. Syntheses, structural variants and characterization of AInM'S₄ (A = alkali metals, Tl; M' = Ge, Sn) compounds; facile ion-exchange reactions of layered NaInSnS₄ and KInSnS₄ compounds. *J. Solid State Chem.* **2016**, 238, 291–302.
- (16) Al-Bloushi, M.; Davaasuren, B.; Emwas, A.-H.; Rothenberger, A. Synthesis and Characterization of the Quaternary Thioaluminogermanates $A(AlS_2)(GeS_2)$ (A = Na, K). Z. Anorg. Allg. Chem. 2015, 641, 1352–1356.
- (17) Ward, M. D.; Pozzi, E. A.; Van Duyne, R. P.; Ibers, J. A. Syntheses, structures, and optical properties of the indium/

- germanium selenides Cs₄In₈GeSe₁₆, CsInSe₂, and CsInGeSe₄. *J. Solid State Chem.* **2014**, 212, 191–196.
- (18) Kumari, A.; Vidyasagar, K. Solid-state synthesis, structural variants and transformation of three-dimensional sulfides, AGaSnS4 (A = Na, K, Rb, Cs, Tl) and Na1.263Ga1.263Sn0.737S4. *J. Solid State Chem.* **2007**, *180*, 2013–2019.
- (19) Hwang, S.-J.; Iyer, R. G.; Trikalitis, P. N.; Ogden, A. G.; Kanatzidis, M. G. Cooling of Melts: Kinetic Stabilization and Polymorphic Transitions in the KInSnSe₄ System. *Inorg. Chem.* **2004**, 43, 2237–2239.
- (20) Hwang, S.-J.; Iyer, R. G.; Kanatzidis, M. G. Quaternary selenostannates $Na_{2-x}Ga_{2-x}Sn_{1+x}Se_6$ and AGaSnSe₄ (A = K, Rb, and Cs) through rapid cooling of melts. Kinetics versus thermodynamics in the polymorphism of AGaSnSe₄. *J. Solid State Chem.* **2004**, 177, 3640–3649.
- (21) Wu, P.; Lu, Y.-J.; Ibers, J. A. Synthesis and structures of the quaternary sulfides KGaSnS₄, KInGeS₄, and KGaGeS₄. *J. Solid State Chem.* **1992**, 97, 383–390.
- (22) Nakamura, Y.; Atsushi, A.; Izumi, N.; Kozo, N. The Crystal Structure of a New Thiosilicate of Thallium, TlInSiS₄. *Bull. Chem. Soc. Jpn.* **1984**, *57*, 1718–1722.
- (23) Nakamura, Y.; Nagashima, K.; Nakai, I. Preparation and characterization of the new quaternary chalcogenides Tl-III-IV-S₄ (III = Al, Ga, In; IV = Si, Ge). *Mater. Res. Bull.* **1984**, 563–570.
- (24) Connelly, N. G.; Damhus, T.; Hartshorn, R. M.; Hutton, A. T. *Nomenclature of Inorganic Chemistry: IUPAC Recommendations* 2005; Royal Society of Chemistry, 2005.
- (25) Liao, J. H.; Varotsis, C.; Kanatzidis, M. G. Syntheses, structures, and properties of six novel alkali metal tin sulfides: K₂Sn₂S₈, alpha-Rb₂Sn₂S₈, beta-Rb₂Sn₂S₈, K₂Sn₂S₅, Cs₂Sn₂S₆, and Cs₂SnS₁₄. *Inorg. Chem.* **1993**, 32, 2453–2462.
- (26) APEX2, version 2014.11-0; Bruker AXS Inst. Inc.: Madison, 2014.
- (27) Spek, A. Single-crystal structure validation with the program PLATON. *J. Appl. Crystallogr.* **2003**, *36*, 7–13.
- (28) Sheldrick, G. M. Cell_Now; Georg-August-Universität: Göttingen, 2012.
- (29) SAINT, version 8.34A; Bruker AXS Inst. Inc.: Madison, 2013.
- (30) TWINABS, version 2012/1; Bruker AXS Inst. Inc.: Madison, 2013.
- (31) Sheldrick, G. SHELXT—Integrated space-group and crystal-structure determination. *Acta Crystallogr., Sect. A: Found. Adv.* **2015**, 71, 3–8.
- (32) Sheldrick, G. M. SHELXL-97—Program for Structures Refinement; University of Göttingen, 1997.
- (33) Balić Žunić, T.; Vickovic, I. IVTON—program for the calculation of geometrical aspects of crystal structures and some crystal chemical applications. *J. Appl. Crystallogr.* **1996**, *29*, 305–306.
- (34) Perdew, J. P.; Burke, K.; Ernzerhof, M. Generalized Gradient Approximation Made Simple. *Phys. Rev. Lett.* **1996**, 77, 3865–3868.
- (35) Kresse, G.; Furthmüller, J. Efficient iterative schemes for ab initio total-energy calculations using a plane-wave basis set. *Phys. Rev.* B **1996**, *54*, 11169–11186.
- (36) Eisenmann, B.; Jakowski, M.; Schäfer, H. Die Strukturen von BaGa₂S₄ und BaAl₂S₄. *Mater. Res. Bull.* **1982**, *17*, 1169–1175.
- (37) Shannon, R. Revised effective ionic radii and systematic studies of interatomic distances in halides and chalcogenides. *Acta Crystallogr., Sect. A: Cryst. Phys., Diffr., Theor. Gen. Crystallogr.* **1976**, 32, 751–767.
- (38) Fard, Z. H.; Kanatzidis, M. G. Phase-Change Materials Exhibiting Tristability: Interconverting Forms of Crystalline α -, β -, and Glassy K2ZnSn3S8. *Inorg. Chem.* **2012**, *51*, 7963–7965.
- (39) Wang, J.; Li, P.; Cai, T.; Yang, D.-D.; Xiong, W.-W. Four two-dimensional ternary selenides based on group 13 and 14 metals: Syntheses, crystal structures, and electrochemical properties. *J. Solid State Chem.* **2018**, 263, 88–93.
- (40) Rubenstein, M.; Roland, G. A monoclinic modification of germanium disulfide, GeS₂. Acta Crystallogr., Sect. B: Struct. Crystallogr. Cryst. Chem. 1971, 27, 505–506.

- (41) Davydyuk, G. E.; Piasecki, M.; Parasyuk, O. V.; Myronchuk, G. L.; Fedorchuk, A. O.; Danylchuk, S. P.; Piskach, L. V.; Mozolyuk, M. Y.; AlZayed, N.; Kityk, I. V. Two-photon absorption of Tl1–xIn1–xSnxSe2 (x=0, 0.1, 0.2, 0.25) single crystalline alloys and their nanocrystallites. *Opt. Mater.* **2013**, *35*, 2514–2518.
- (42) Myronchuk, G.; Danylchuk, S.; Parasyuk, O. V.; Piskach, L. V.; Fedorchuk, A. O. Spectral and conductivity features of novel ternary Tl1-xln1-xSnxS2 crystals. *Cryst. Res. Technol.* **2013**, *48*, 464–475.
- (43) Mozolyuk, M. Y.; Piskach, L. V.; Fedorchuk, A. O.; Kityk, I. V.; Olekseyuk, I. D.; Parasyuk, O. V. Phase diagram of the quasi-binary system TlInSe2—SnSe2. *J. Alloys Compd.* **2011**, *509*, 2693—2696.
- (44) Zamurueva, O. V.; Myronchuk, G. L.; Lakshminarayana, G.; Parasyuk, O. V.; Piskach, L. V.; Fedorchuk, A. O.; AlZayed, N. S.; El-Naggar, A. M.; Kityk, I. V. Structural and optical features of novel Tl1–xln1–xGexSe2 chalcogenide crystals. *Opt. Mater.* **2014**, *37*, 614–620
- (45) Liu, Q.-Q.; Liu, X.; Chen, L.; Wu, L.-M. AGaSnS4 (A = Rb, Cs): Three sulfides and their structure diversity. *J. Solid State Chem.* **2020**, 285, No. 121233.
- (46) Bärnighausen, H. Group-subgroup relations between space groups as an ordering principle in crystal chemistry: the "family tree" of perovskite-like structures. *Acta Crystallogr., Sect. A* **1975**, *31*, No. 01.1-9.
- (47) Mucha, I. Phase diagram for the quasi-binary thallium(I) selenide-indium(III) selenide system. *Thermochim. Acta* **2012**, 550, 1–4
- (48) Abudurusuli, A.; Wu, K.; Li, J.; Yalikun, A.; Yang, Z.; Pan, S. LiBa2MIIIQ4 (MIII = Al, Ga, In; Q = S, Se): A Series of Metal Chalcogenides with a Structural Transition. *Inorg. Chem.* **2019**, *58*, 12859–12866.